Journal of Applied Research in Water and Wastewater
E-ISSN: 2476-6283
Journal homepage: https://arww.razi.ac.ir

Fe/Ti-codoped strontium oxide nanoparticles for enhanced photocatalytic degradation of methyl orange

Muhammad Kashif[1], Muhammad Jawad[1], Azmat Ali Khan[1], Hao Sun[2,3], Khair Ullah[1], Olayemi J Fakayode[4], Shohreh Azizi*[,4]

[1]Department of Chemistry, Abdul Wali khan University, Mardan, Pakistan.
[2]Faculty of Science, Autonomous University of Madrid, Spainish National Research Council (UAM-CSIC), Madrid, Spain.
[3]Cantoblanco Campus, Consejo Superiorde Investigaciones Científicas, CSIC, Madrid, Spain.
[4]UNESCO-UNISA Africa Chair in Nanosciences/Nanotechnology, College of Graduate Studies, University of South Africa, Muckleneuk Ridge, Pretoria, South Africa.

GRAPHICAL ABSTRACT

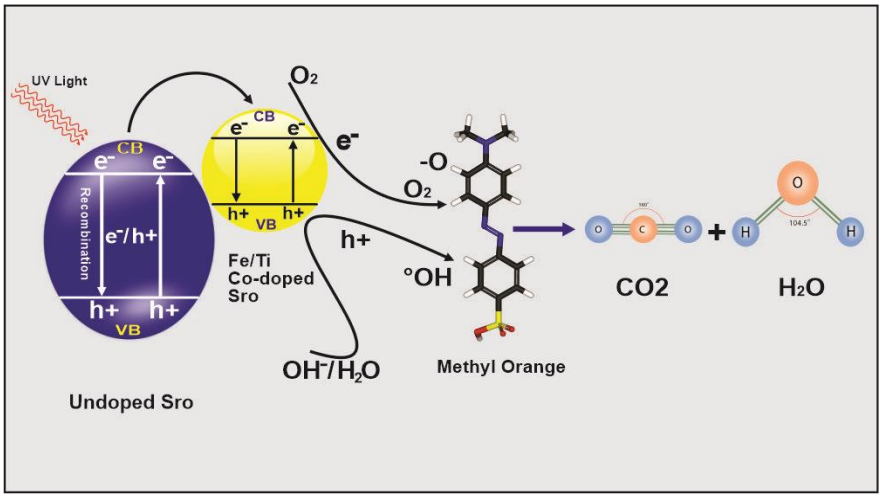

ARTICLE INFO

Type of Article:
Research Article

Article history:
Received 14 April 2024
Received in revised form 2 June 2024
Accepted 4 June 2024
Available online 5 June 2024

Keywords:
Fe/Ti
Co-doped
Strontium oxide
Photocatalysis
Methyl orange

ABSTRACT

This study presents a method for enhancing the photocatalytic properties of strontium oxide (SrO) nanoparticles (NPs) through doping with Iron (Fe) and titanium (Ti) ions using hydrothermal synthesis. The materials were characterized using a range of spectroscopic and microscopic techniques to ensure accurate analysis of their structure and composition. Photocatalytic efficiencies of the as-synthesized materials were evaluated against the degradation of methyl orange dye, achieving about 98 % removal in 90 min with 3 % doped material. The degradation efficiency was found to be dependent on several factors including pH, initial dye concentration, and catalyst dosage. Optimal conditions were determined to be a pH of 4, an initial dye concentration of 20 mg/L, and a catalyst dosage of 150 mg. These findings suggest that the Fe/Ti-codoped SrO nanoparticles hold significant potential for applications in environmental cleanup processes, particularly in the degradation of organic pollutants. The study provides valuable insights into the synthesis and application of doped nanoparticles in photocatalysis, highlighting their efficiency and the importance of optimizing reaction conditions to maximize performance.

1. Introduction

Nanoparticles (NPs) hold significant promise for diverse applications across scientific disciplines, encompassing medicine (Zhang *et al.*, 2008), environmental remediation (Das *et al.*, 2022), electronics (Tan *et al.*, 2019), construction materials (Mohajerani *et al.*, 2019), energy conservation (Tabassum *et al.*, 2019), catalysis, green chemistry (Kalidindi and Jagirdar, 2012), sustainable agriculture (Hazarika *et al.*, 2022), and antimicrobial science (Sun, Qiu, and Liang, 2008; Wang *et al.*, 2009; Dizaj *et al.*, 2014). Notably, there has been a growing

*Corresponding author Email: azizis@unisa.ac.za, shohrehazizi1379@gmail.com

Cite this article: M. Kashif, M. Jawad, A. Ali Khan, H. Sun, Khair Ullah, T. Ahmad, O. J Fakayode, S. Azizi, Fe/Ti-codoped strontium oxide nanoparticles for enhanced photocatalytic degradation of methyl orange, Journal of Applied Research in Water and Wastewater, 11 (1), 2024, 8-14. doi: https://doi.org/10.22126/arww.2024.10753.1336

utilization of metal oxides-based materials, such as ZnO (Zada *et al.*, 2022), V_2O_5 (Jenifer *et al.*, 2021), CuO (Sasikala *et al.*, 2016), TiO_2 (Al-Mamun *et al.*, 2022), WO_3 (Verma, Singh, and Kumar, 2020), Fe_2O_3 (Subaihi and Naglah, 2022), SnO_2 (Mishra, Biswal, and Sahu 2022), Al_2O_3 (Anbarasu *et al.*, 2020), and ZrO_2 (Dawoud *et al.*, 2020), in the realm of photocatalysis. While titanium dioxide (TiO_2) has demonstrated efficacy as a catalyst in the degradation of dye compounds under UV irradiation, its limited visible light absorption presents a challenge when paired with renewable energy sources like solar energy system. The unique characteristics of nanoparticles, stemming from their significantly higher surface-to-volume ratio, distinguish them from their bulk counterparts. The discernible escalation in nanomaterial production, particularly attributed to their capacity for enhancing catalytic reaction efficiencies at the nanoscale level, is evident (Hanafi and Sapawe, 2020).

Methyl orange (MO) is an acidic and ionic water-soluble azo dye known to possess carcinogenic properties, capable of inducing nausea and diarrhoea in humans, and potentially leading to fatality in high concentrations. Due to its high water solubility, it presents challenges in water removal (Hanafi and Sapawe, 2020). With a chemical formula of $C_{14}H_{14}N_3O_3SNa$ and a molecular weight of 327.33 g/mol, MO exhibits an absorption spectrum with a characteristic wavelength of 465 nm. When dissolved in an aqueous solution, the MO exists in a basic form (Darwish, Rashad, and AL-Aoh, 2019), transitioning to a red hue under increased acidity. The presence of an azo group (N=N) in its structure renders MO resistant to biodegradation, primarily attributed to the difficulty in breaking the N=N bond (Sinha and De, 2020).

Organic dye degradation with pure metallic NPs is a common study. Doping, on the other hand, inserts defects into the perfect crystal lattice of the native semiconductor while also improving catalytic activity by changing the electrical structure. Defects of this type can trap electrons or holes generated during the photoexcitation process. Another significant role of the defect sites such as vacancy generation is to increase the catalytic activation of strong bonds, thus aiding the process kinetically. Doping may also result in the formation of an extra charge carrier in the photocatalyst, which may narrow or widen the original bandgap. As a result, doping can vary light absorption, limit recombination trap sites, and alter photocatalytic activity toward a substrate.

Strontium oxide (SrO) is acknowledged as a highly effective catalyst for transesterification and is regarded as one of the most promising alkaline earth metal oxides for deployment as a heterogeneous-based catalyst. Research has demonstrated its superior catalyst activity compared to calcium and magnesium oxides (Lee *et al.*, 2020). However, its usage is impeded by the challenging preparation and size control, leading to economic manufacturing difficulties. To mitigate this limitation, ongoing research endeavors are focused on the synthesis of SrO nanoparticles using methodologies such as wet bio-reduction and hydrothermal techniques. Nanoparticles hold potential applications in diverse domains including gas electrodes, lithium-ion batteries, semiconductors, and supercapacitors (Khalil *et al.*, 2022). Furthermore, modified iterations of SrO nanoparticles, encompassing doped, co-doped, and other modified forms such as ZnO/SrO, TiO_2/SrO, and SrO/$CuBi_2O_4$, exhibit promising effects in photocatalytic dye degradation (Harish *et al.*, 2017; Ikram *et al.*, 2021; Ikram *et al.*, 2022). Additionally, strontium oxide nanoparticles demonstrate potential in biological applications such as bone tissue engineering, antimicrobial coatings, as well as, optoelectronics, energy storage, environmental remediation, and catalysis.

Hydrothermal synthesis represents a widely employed method for the production of nanoparticles via a solution-based reaction approach. This method accommodates a broad spectrum of temperatures, extending from ambient to elevated levels. The resultant nanomaterial's morphology is amenable to manipulation through the application of either high-pressure or low-pressure conditions, contingent upon the vapour pressure of the primary composition involved in the reaction. The hydrothermal approach confers the distinct advantage of enabling precise control over grain size, crystalline phase, particle morphology, and surface chemistry by modulating the solution composition, reaction temperature, pressure, solvent properties, additives, and aging duration. Furthermore, this method facilitates the production of nanomaterials that exhibit instability at heightened temperatures, enabling high vapour pressure materials to be synthesized with minimal material loss (Liu *et al.*, 2014; Darr *et al.*, 2017, Yang and Park, 2019). The present investigation successfully synthesizes Fe/Ti co-doped SrO nanoparticles using a hydrothermal approach. The study includes pure SrO nanoparticles (S) and those co-doped with 2% (S2), 3% (S3), and 4% (S4) Fe/Ti, characterizing and assessing their effectiveness in the photocatalytic degradation of methyl orange dye. Remarkably, the doped nanocomposites demonstrated superior photocatalytic degradation of methyl orange compared to pristine SrO nanoparticles. This novel approach highlights the significant potential of these nanocomposite particles in environmental remediation, providing a promising solution for industrial wastewater treatment.

2. Materials and methods

2.1. Chemicals and equipment

Iron chloride and strontium nitrate were procured from Daejung, South Korea. The chemicals titanium nitrate, sodium hydroxide, and methyl orange dye were acquired from Sigma-Aldrich. In this study, a Teflon-lined autoclave with a capacity of 10 mL (Model: Tob new energy, Item No: Tob reactor, China) was employed. The autoclave was constructed using stainless steel and designed to withstand operating temperatures of up to 240 °C. Additionally, a muffle furnace (manufactured by Across International) capable of reaching temperatures as high as 1300°C was utilized for heating, drying, and calcination of the samples.

2.2. Synthesis of Fe and Ti co-doped strontium oxide NPs

The hydrothermal technique was employed to synthesize SrO NPs and their co-doped forms. To make the solution for the synthesis of NPs, 3 grams of strontium nitrate hexahydrate were dissolved in 75 mL of deionized water. Three different solutions of pure titanium and iron chloride were prepared and added to three different solutions of strontium nitrate. Stirring was done continuously at room temperature until the solution became a homogenous mixture. The mixture was then mixed with 10 % sodium hydroxide solution gradually, maintaining a basic pH of 10. As a result, a white precipitate was formed. The precipitate was resolved, and a mixture was created. The homogeneous mixture was put into a stainless steel autoclave lined with Teflon and heated to high temperature and pressure to produce a precipitate. The autoclave with the solution inside was then placed in an oven that was preheated to 170°C for 10 hrs. After the autoclave cooled down, the precipitate went through a washing and centrifugation procedure to remove any untreated reactants. The precipitate was dried at 120°C and then heated to 460 °C for 60 min of calcination, producing both undoped and doped SrO (S (0 % Fe/Ti), S2 (2% Fe/Ti), S3 (3% Fe/Ti), and S4 (4% Fe/Ti)).

2.3. Characterization

Several characterization techniques were taken into consideration to evaluate and understand the characteristics of the samples. To facilitate absorbance measurements, a UV-Vis spectroscopic investigation was carried out using a Shimadzu UV-1800 spectrometer, covering a wavelength range of 190-1100 nm. The FT-IR (V. 640, USA) instrument, which operates in the wavenumber range of 400 to 4000 cm^{-1}, was used to analyze the functional groups. A 0.09 g sample served as the basis for the generation of spectra. Photoluminescence (PL) analysis was used to determine the emission properties of the materials. This analysis uses a non-destructive method and covers a spectral range of 230 to 1000 nm. Utilizing the D-2 Phaser X-ray diffractometer (Burker, Denver, CO, USA), 20 degrees per minute of scanning was done. To obtain information about the crystalline structure of the samples, a copper kα radiation source was employed. A scanning electron microscope (model JSM5910, JEOL, Kyoto, Japan) was used to evaluate the morphology of the samples. A voltage of 30 KV was used accordingly. The elemental compositions of the samples were ascertained by employing the EDX technique, which operates in the energy range of 0-14 keV.

2.4. Photocatalytic degradation of methyl orange dye

To conduct the photo-catalytic experiment, a 100-volt lightbulb was used. Briefly, a 120 mL methyl orange solution with 25 parts per million (mg/L) concentration was mixed with a dispersion of the photo-catalysts. The resulting solution was stirred at room temperature for 25 min without light to achieve an adsorption/desorption equilibrium. The combination was then subjected to irradiation while being vigorously stirred. To confirm that all solid catalysts had been completely removed, an aliquot of about 4-5 mL of the solution was taken out and centrifuged regularly. In the end, a UV-visible spectrometer was used to evaluate the catalyst's effectiveness in the dye degradation. The formula used to calculate the percent degradation is given in Eq. 1.

$$\text{Degradation (\%)} = (C_0\text{-}C_t) / C_0 \times 100 \quad (1)$$

where, C_0 and C_t denote the dye concentrations before and after photoirradiation.

3. Results and discussion

3.1. Material evolution, UV-Vis, FTIR and PL characterization

Both doped and undoped SrO materials were acquired in the form of dried powders. The optical, surface functional group and crystallinity characteristics of the materials were assessed using UV-visible spectroscopy, FTIR, XRD, and photoluminescence techniques. The UV-Vis spectrum of the as-synthesized materials is presented in Fig. 1a. Notably, the Sr-O nanomaterial exhibited an absorption peak at 290 nm, indicating a band gap of approximately 4.28 eV. The introduction of Fe and Ti into the mixture resulted in a gradual expansion of the absorption edges towards longer wavelengths, leading to a reduction in band gaps. Remarkably, SrO nanocrystals doped with 2%, 3%, and 4% concentrations of Fe and Ti displayed absorption edges at approximately 310 nm, 316 nm, and 324 nm, respectively. The findings from the photoluminescence analysis are depicted in Fig. 1b. It is evident that doping led to a blue shift in the emission wavelength and enhanced photoluminescence intensity, with S2 exhibiting the highest intensity, followed by S4 and S3, which exhibited the lowest intensity. This behaviour suggests that S3 has the potential to most effectively reduce the recombination of holes and electrons.

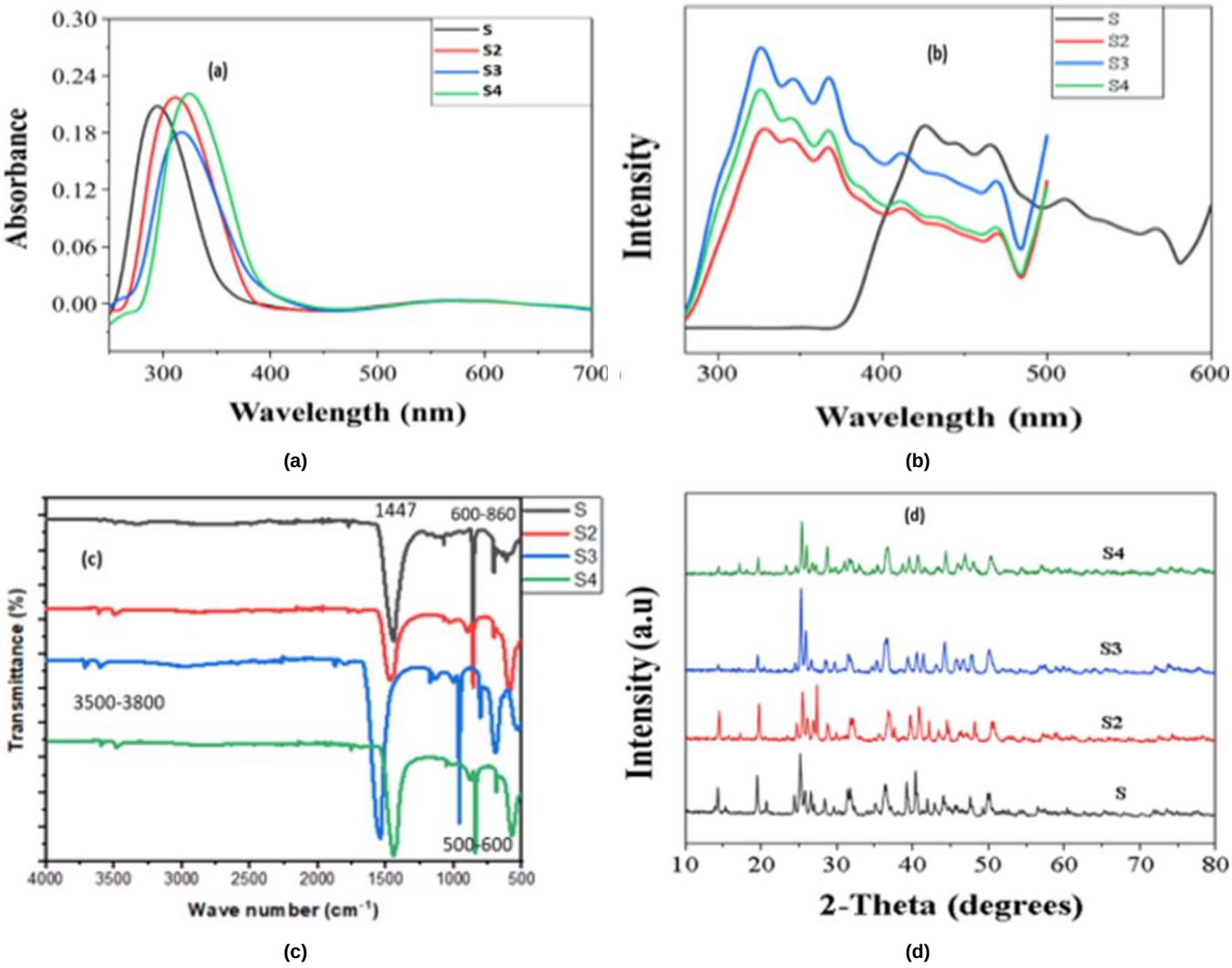

Fig. 1. Optical and crystallinity characterization of the as-synthesized materials. (a) UV-Vis; (b) Photoluminescence spectra; (c) FTIR spectra; (d) XRD spectra.

The findings of the FTIR analysis are illustrated in Fig. 1C. In the Fig., the spectral peaks observed within the range of 600-860 cm^{-1} are attributed to the un-doped Sr-O stretching (Athar, 2013). Furthermore, a discernible peak at 1447 cm^{-1} signifies the H-O-H bending. Additionally, the presence of the -OH group is indicated by a peak identified within the wavenumber region of 3800 cm^{-1} to 3500 cm^{-1}. The observed blue shift of the 1447 cm^{-1} peak in conjunction with increased dopant levels from 0% to 3%, and the overall enhancement of peaks within the 500-800 cm^{-1} range with doping, are visually evident in Fig. 1c. The X-ray diffraction (XRD) analysis results are depicted in Fig. 1d. As shown in Fig. 1d, distinctive peaks in the spectrum of undoped SrO, corresponding to crystal planes (101), (112), (100), (200), (202), (114), (213), (222), (310), (312), (111), (332), (431), (240), and (161) at 2-theta angles of 14.29°, 19.53°, 20°, 24.41°, 25.19°, 28.39°, 31.78°, 35.10°, 36.40°, 39.23°, 40°, 41°, 44°, 47°, and 50°, respectively. The observed narrow and sharp peaks suggest a high-quality crystalline nature of the samples. Furthermore, peaks were assigned based on JCPDS file numbers (JCPDS file#6-520) (Aghaee and Manteghi, 2022). Notably, the introduction of Fe and Ti as dopants led to enhanced crystal planes (202), (310), and (161). Subsequently, a significant increase in the intensity of the XRD peak at 25.19° was observed. Additionally, the determination of the crystallite size using Scherer's equation revealed average diameters of 33 nm, 35 nm, 28 nm, and 29 nm for undoped SrO NPs and doped SrO NPs with 2%Fe/Ti, 3%Fe/Ti, and 4%Fe/Ti, respectively. It is evident that these samples share similar sizes, with no discernible alteration in the XRD pattern. Moreover, Fig. 1d demonstrates a proportional increase in XRD peak intensity with the rise in the concentration of Fe and Ti dopants, with the exception of S4, which exhibits reduced intensity relative to S3.

3.2. SEM and EDX analysis

The results of the morphology analysis of the as-synthesized materials show the evolution of aggregated spherical-shaped structures as shown in Fig. 2.a and 2.b. Notably, doping did not induce a change in the pristine SrO morphology. However, the EDX analysis confirmed the presence of Sr, O, Fe, and Ti in the as-synthesized materials (Fig. 3).

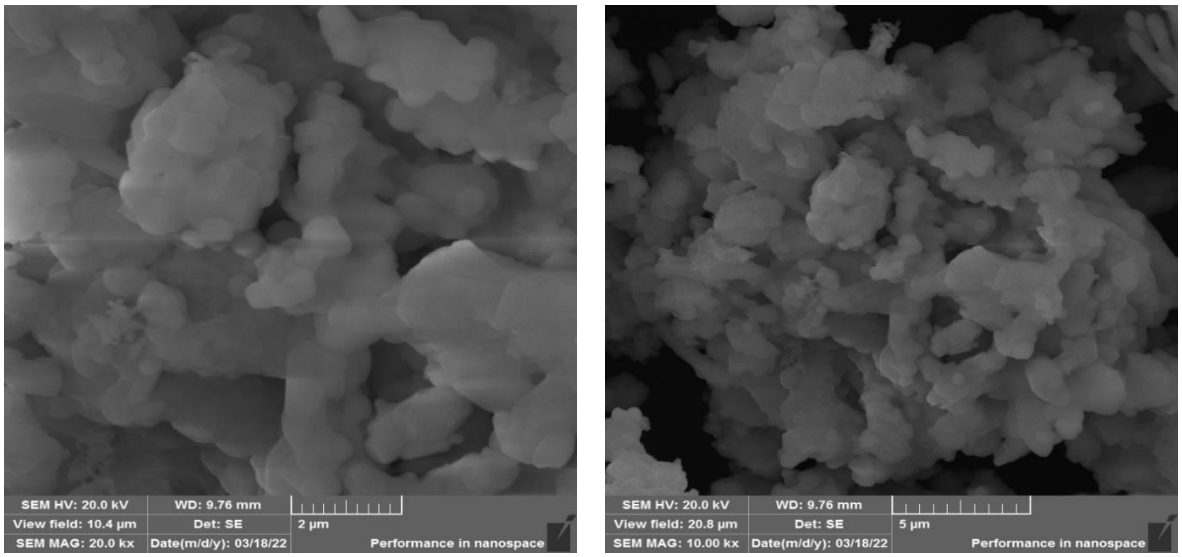

(a) **(b)**

Fig. 2. (a) SEM images of (a) 2% Fe/Ti co-doped SrO nanoparticles and (b) 2% Fe/Ti co-doped SrO nanoparticles.

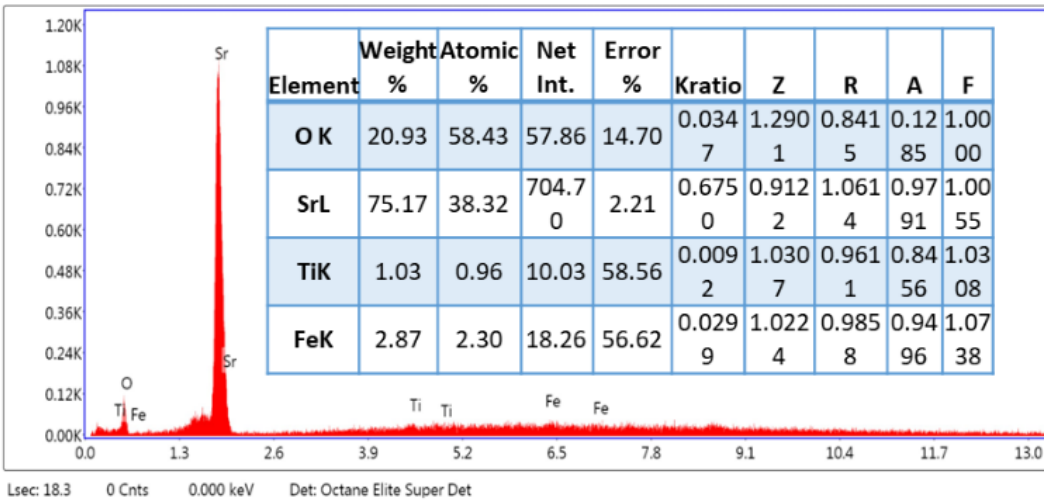

Element	Weight %	Atomic %	Net Int.	Error %	Kratio	Z	R	A	F
O K	20.93	58.43	57.86	14.70	0.0347	1.2901	0.8415	0.1285	1.0000
SrL	75.17	38.32	704.70	2.21	0.6750	0.9122	1.0614	0.9791	1.0055
TiK	1.03	0.96	10.03	58.56	0.0092	1.0307	0.9611	0.8456	1.0308
FeK	2.87	2.30	18.26	56.62	0.0299	1.0224	0.9858	0.9496	1.0738

Fig. 3. EDX spectrum of the as-synthesized material.

3.3. Photocatalytic degradation

To conduct the photocatalytic experiment, a 100-volt lightbulb illuminated a 120 mL methyl orange solution at 25 mg/L concentration, mixed with photocatalysts. The mixture was stirred for 25 min in the dark to reach adsorption/desorption equilibrium, then exposed to light while stirring. Samples were centrifuged to ensure the removal of solid catalysts, and a UV-visible spectrometer measured the dye degradation efficiency. Fig. 4a-d shows the results of the photodegradation using the doped and undoped SrO at the different experimental conditions. Since pure SrO has a large band gap and a fast rate of charge recombination, it was not surprising that its photocatalytic activity was on the low end compared to those of the doped materials. The S3 material has the highest degree of degradation efficiency, while a decrease in activity was noticed with S4. As shown in Fig. 4a, the photodegradation increases with time and seems to level up at some time, mostly after 90 min for S3 and 150 min for other materials, i.e. the S, S2 and S4. Also, the optimal dosage for all materials was 150 mg as revealed in Fig. 4b. The results of the effects of the initial concentration and pH on the degradation efficiency showed that both degradation decreased with increasing initial concentration and pH (Fig. 4c-d). Decreasing photocatalytic activity with higher photocatalyst loading up to 150 mg is due to light scattering and shielding effects, which limit photon penetration and electron-hole pair generation. High MO concentration and high alkalinity reduce light penetration and alter surface charge interactions, diminishing dye adsorption and photocatalytic efficiency.

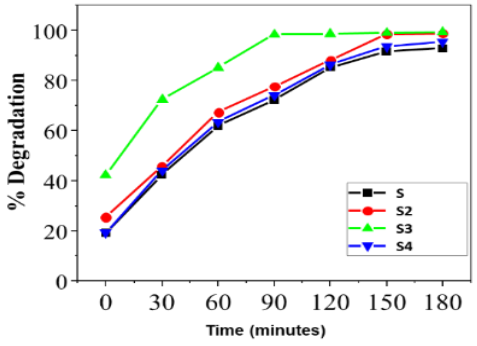

(a)

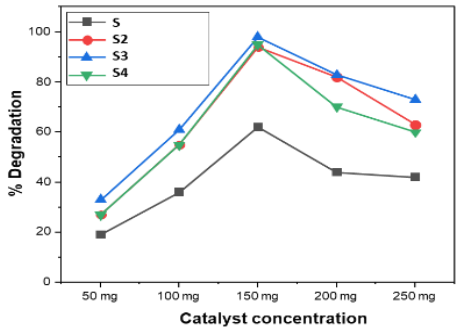

(b)

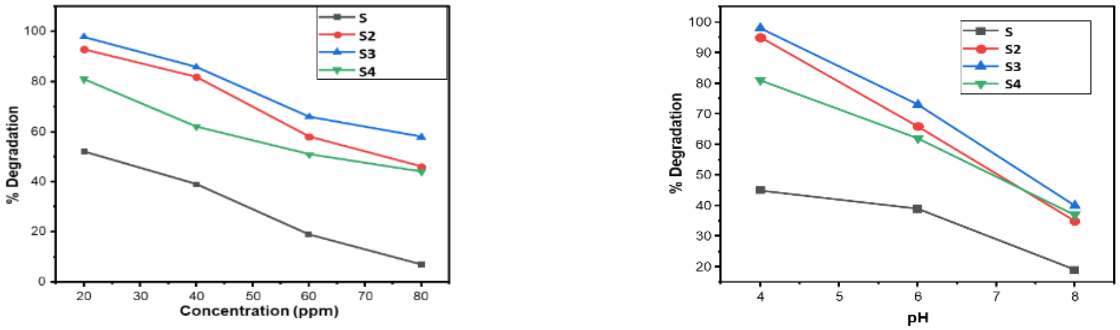

(c) (d)

Fig. 4. Photodegradation of S, S2, S3, and S4 under different experimental conditions. (a) Time variation ;(b) catalyst dosage; (c) initial concentration; (d) pH variation.

3.4. Mechanism of photocatalytic degradation

Fig. 5 depicts a plausible photocatalysis mechanism for the degradation of the MO dye. The initial step involves the adsorption of dye molecules onto the catalyst's surface. Upon incidence of light on the photocatalyst, the absorption of a photon (light energy) leads to the separation of the electron (e^-) and holes (h^+). The efficiency of this process is contingent on the energy of the incident light relative to the photocatalyst's band gap. When the energy of the incident light surpasses the band gap of the photocatalyst, electrons (e^-) transit from the valence band (VB) to the conduction band (CB), leaving holes in the valence band. As illustrated in Fig. 4, the electrons in the conduction band can freely interact with oxygen, giving rise to the formation of superoxide anion, a potent oxidizing agent that facilitates the conversion of dye molecules to CO_2 and H_2O (Slimani *et al.*, 2023). Conversely, the holes can oxidize water to hydroxyl radicals, which further contributes to the conversion of the dye to CO_2 and H_2O (Al-Mamun *et al.*, 2023). The incorporation of transition metals into the semiconductor lattice, such as that of SrO, serves to enhance the separation of charge carriers and thus prevents the recombination of photoinduced electrons and holes. The photocatalytic process can be summarized through a series of chemical reactions outlined in Eqs. 2-7 below:

$$SrO + hv \rightarrow SrO\ (ecb^- + hvb+) \quad (2)$$
$$SrO\ (ecb^- + hvb+) + O_2/OH^-/H_2O \rightarrow {}^{\circ}OH + O_2{}^{\circ-} \quad (3)$$
$$(Fe/Ti)^{+n} + ecb^-\ (CB) \rightarrow (Fe/Ti)^{+n-1}\ (\text{electron trap}) \quad (4)$$
$$(Fe/Ti)^{+n-1} + O_2 \rightarrow (Fe/Ti)^{+n} + O_2{}^{\circ-}\ (\text{electron release}) \quad (5)$$
$$hvb+\ (VB) + OH^-/H2O \rightarrow {}^{\circ}OH \quad (6)$$
$$^{\circ}OH/\ O_2{}^{\circ-} + MO\ \text{dye} \rightarrow \text{degraded products} + CO_2 + H_2O \quad (7)$$

Table 1 shows the comparison of the effectiveness of the present work with some works reported in the literature on MO degradation. The details of each material and photocatalytic efficiency in terms of % removal are mentioned. It is evident that the prepared samples, S, S2, S3 and S4, have remarkable degradation capability compared to most of those of the previously reported works in terms of timing and degradation efficiency.

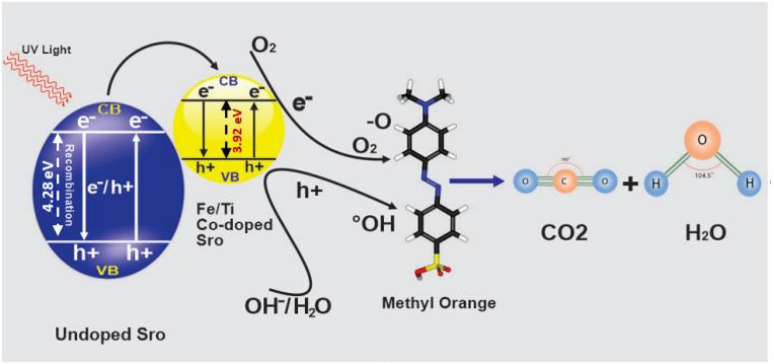

Fig. 5. Proposed reaction mechanism of MO dye degradation.

Table 1. Comparison of the present work with literature reports on MO's degradation.

NPs and nanocomposites	Method of preparation	Morphology	Time for degradation, min	Removal, %	Ref.
S	Hydrothermal	Spherical	150	150 and 90	This work
S2	Hydrothermal	Spherical	150	150 and 98.48	This work
S3	Hydrothermal	Spherical	90	90 and 98.27	This work
S4	Hydrothermal	Spherical	150	150 and 93.52	This work
NiO	Green synthesis	Spherical	30	30 and 90	Barzinjy *et al.*, 2020
CBMO	Co-precipitation	porous	120	120 and 74	Makeswari and Saraswathi, 2020
TiO_2	Hydrothermal	Tube and Rod	180	180 and 45	Raliya *et al.*, 017)
ZnO	Sol-gel	Nano rods	180	180 and 57	Tran *et al.*, 2021
GO	Hummer's technique	Nano-sheets	180	180 and 53.8	Raliya *et al.*, 2017
Co_3O_4-ZnO	In-situ	Rhombic dodecahedral	120	120 and 76.8	Tran *et al.*, 2021
Fe_3O_4	Green synthesis	Spherical	360	360 and 98.6	Kouhbanani *et al.*, 2018
Al/ZnO	Sol-gel	Spherical	40	40 and 99	Peerakiatkhajohn *et al.*, 2021
Fe-TiO_2	Controlled hydrolysis	Spherical	360	360 and 79	Tong *et al.*, 2008
SO_2-4-TiO_2	Sol-gel	Mesoporous	240	240 and 61	Parida *et al.*, 2008

ZnO-PVP	In-situ	Agglomerated	120 and 82	Khan, Naeem, and Mahmood, 2020a
CuO/NC	Chemical reduction	Agglomerated	4 and 97.18	Khan *et al.*, 2020b
Ag-$GdFeO_3$	Photo-assisted Deposition	Spherical	60 and 98	Baeissa, 2016
FA/CuO	Green synthesis	Spheroidal	40 and 99	Mazumder and Rano, 2018
Fe_3O_4	Co-precipitation	Spherical	110 and 98.3	Al-Abdallat *et al.*, 2019
CeO_2-Fe_2O_3	Thermal decomposition	Agglomerated	120 and 93.8	Krishnan *et al.*, 2021

4. Conclusions

Strontium oxide (SrO) and Fe/Ti co-doped SrO nanoparticles were synthesized utilizing a hydrothermal process. The photocatalytic efficiencies of the materials were evaluated against the degradation of methyl orange dye. A % removal of about 98 % was achieved within 90 min of interaction using 3% Fe/Ti co-doped SrO nanomaterials. The current approach shows the potential of using SrO co-doped with Fe and Ti as efficient nanomaterials for the photocatalytic degradation of methyl orange dye in water.

Author Contributions

Muhammad Kashif: Conceptualization, methodology, and writing original draft preparation.
Muhammad Jawad: Synthesis of Ni/Zn co-doped strontium oxide nanoparticles via hydrothermal method.
Azmat Ali Khan: Characterization and analysis of photocatalytic properties.
Hao Sun: Experimental design and data interpretation.
Khair Ullah: Project administration.
Olayemi J Fakayode: Mathematical calculation and synthesis.
Shohreh Azizi: Supervision and conceptualization.

Conflict of Interest

The authors declare that they have no known competing financial interests or personal relationships that could have appeared to influence the work reported in this paper.

Acknowledgments

The author is greatly acknowledging the Department of Chemistry, Abdul Wali khan University Mardan and Government Postgraduate College Nowshera, Khyber Pakhtunkhwa, Pakistan for providing experimental facilities.

Data Availability Statement

The data that support the findings of this study are available from the author, Muhammad Kashif, upon reasonable request. Due to privacy concerns, the data are not publicly available.

References

Aghaee, M., and Manteghi, F. (2022) 'Antibacterial activity of Ag_2O/SrO/CaO nanocomposite' *Chemistry Proceedings*, *12* (1), p. 77. doi: https://doi.org/10.3390/ecsoc-26-13577

Al-Abdallat, Y. *et al.* (2019) 'Photocatalytic degradation dynamics of methyl orange using coprecipitation synthesized Fe_3O_4 nanoparticles', *Water, Air, & Soil Pollution*, *230*, pp. 1-16. doi: https://doi.org/10.1007/s11270-019-4310-y.

Al-Mamun, M. R. *et al.* (2022) 'Synthesis, characterization, and photocatalytic performance of methyl orange in aqueous TiO_2 suspension under UV and solar light irradiation', *South African Journal of Chemical Engineering*, *40* (1), pp. 113-125. doi: https://doi.org/10.1016/j.sajce.2022.02.002

Al-Mamun, M. R. *et al.* (2023) 'Enhanced photocatalytic activity of Cu and Ni-doped ZnO nanostructures: A comparative study of methyl orange dye degradation in aqueous solution', *Heliyon*, *9* (6), p. e16506. doi: https://doi.org/10.1016/j.heliyon.2023.e16506.

Anbarasu, S. *et al.* (2020) 'Visible light mediated photocatalytic activity of Ni-doped Al_2O_3 nanoparticles', *Surfaces and Interfaces*, 18, p. 100416. doi: https://doi.org/10.1016/j.surfin.2019.100416

Athar, T. (2013) 'Synthesis and characterization of strontium oxide nanoparticles via wet process', *Materials Focus*, *2*(6), pp. 450-453. doi: https://doi.org/10.1016/j.surfin.2019.100416/10.1166/mat.2013.1121

Baeissa, E. S. (2016) 'Environmental remediation of aqueous methyl orange dye solution via photocatalytic oxidation using $AgGdFeO_3$ nanoparticles' *Journal of Alloys and Compounds*, *678*, pp. 267-272. doi: https://doi.org/10.1016/j.jallcom.2016.04.007

Barzinjy, A. A., *et al.* (2020) 'Green and eco-friendly synthesis of Nickel oxide nanoparticles and its photocatalytic activity for methyl orange degradation', *Journal of Materials Science: Materials in Electronics*, *31* (14), pp. 11303-11316. doi: https://doi.org/10.1007/s10854-020-03679-y.

Darr, J. A. *et al.* (2017) 'Continuous hydrothermal synthesis of inorganic nanoparticles: applications and future directions', *Chemical Reviews*, *117*(17), pp. 11125-11238. doi: https://doi.org/10.1021/acs.chemrev.6b00417

Darwish, A. A. A., Rashad, M., and AL-Aoh, H. A. (2019) 'Methyl orange adsorption comparison on nanoparticles: Isotherm, kinetics, and thermodynamic studies', *Dyes and Pigments*, *160*, pp. 563-571. doi: https://doi.org/10.1016/j.dyepig.2018.08.045

Das, P. K. *et al.* (2022). Nanoparticle assisted environmental remediation: Applications, toxicological implications and recommendations for a sustainable environment. *Environmental Nanotechnology, Monitoring & Management*, *18*, p. 100679. doi: https://doi.org/10.1016/j.enmm.2022.100679

Dawoud, T. M. *et al.* (2020) 'Photocatalytic degradation of an organic dye using Ag doped ZrO_2 nanoparticles: Milk powder facilitated eco-friendly synthesis,' *Journal of King Saud University-Science*, *32*(3), pp. 1872-1878. doi: https://doi.org/10.1016/j.jksus.2020.01.040

Dizaj, S. M. *et al.* (2014) 'Antimicrobial activity of the metals and metal oxide nanoparticles', *Materials Science and Engineering: C*, *44*, 278-284. doi: https://doi.org/10.1016/j.msec.2014.08.031

Hanafi, M. F., and Sapawe, N. (2020) 'An overview of recent developments on semiconductor catalyst synthesis and modification used in photocatalytic reaction', *Materials Today: Proceedings*, *31*, pp. A151-A157. doi: https://doi.org/10.1016/j.matpr.2021.01.262

Harish, S. *et al.* (2017) 'Synthesis of ZnO/SrO nanocomposites for enhanced photocatalytic activity under visible light irradiation', *Applied surface science*, *418*, pp. 147-155. doi: https://doi.org/10.1016/j.apsusc.2017.01.164

Hazarika, A., *et al.* (2022). An overview of the role of nanoparticles in sustainable agriculture. *Biocatalysis and Agricultural Biotechnology*, *43*, p. 102399. doi: https://doi.org/10.1016/j.bcab.2022.102399

Ikram, M. *et al.* (2021) 'Efficient dye degradation, antimicrobial behavior and molecular docking analysis of gold (Au) and cellulose nanocrystals (CNC)-doped strontium oxide nanocomposites', *Journal of Nanostructure in Chemistry*, pp. 1-18. doi: https://doi.org/10.1007/s40097-021-00452-3

Ikram, M. *et al.* (2022) 'Facile synthesis of starch and tellurium doped SrO nanocomposite for catalytic and antibacterial potential: In silico molecular docking studies', *International Journal of Biological Macromolecules*, *221*, pp. 496-507. doi: https://doi.org/10.1016/j.ijbiomac.2022.09.034

Jenifer, A., Sastri, M. S., and Sriram, S. (2021) 'Photocatalytic dye degradation of V_2O_5 nanoparticles—An experimental and DFT analysis', *Optik*, *243*, p. 167148. doi: https://doi.org/10.1016/j.ijleo.2021.167148

Kalidindi, S. B., and Jagirdar, B. R. (2012) 'Nanocatalysis and prospects of green chemistry', *ChemSusChem*, *5*(1), pp. 65-75. doi: https://doi.org/10.1002/cssc.201100377

Khalil, K. D., *et al.* (2022) 'Chitosan-strontium oxide nanocomposite: preparation, characterization, and catalytic potency in thiadiazoles synthesis', *Polymers*, *14*(14), p. 2827. doi: https://doi.org/10.3390/polym14142827

Khan, A., Naeem, A., and Mahmood, T. (2020a) 'Kinetic studies of methyl orange and Congo red adsorption and photocatalytic degradation onto PVP-functionalized ZnO', *Kinetics and Catalysis*, *61*, pp. 730-739. doi: https://doi.org/10.1134/S0023158420050055

Khan, I. *et al.* (2020b) 'Nanoclay-mediated photocatalytic activity enhancement of copper oxide nanoparticles for enhanced methyl orange photodegradation', *Journal of Materials Science: Materials in Electronics*, *31*, pp. 8971-8985. doi: https://doi.org/10.1007/s10854-020-03431-6

Kouhbanani, M. A. J. *et al.* (2018) 'Green synthesis of iron oxide nanoparticles using Artemisia vulgaris leaf extract and their application as a heterogeneous Fenton-like catalyst for the degradation of methyl orange', *Materials Research Express*, *5*(11), p. 115013. doi: https://doi.org/10.1088/2053-1591/aadde8

Krishnan, A. *et al.* (2021) 'Tuning of photocatalytic performance of CeO_2-Fe_2O_3 composite by Sn-doping for the effective degradation of methlene blue (MB) and methyl orange (MO) dyes', *Surfaces and Interfaces*, *22*, p. 100808. doi: https://doi.org/10.1016/j.surfin.2020.100808

Lee, H. *et al.* (2020) 'Heterogeneous catalysts using strontium oxide agglomerates depositing upon titanium plate for enhancing biodiesel production,' *Catalysts*, *11*(1), p. 30. doi: https://doi.org/10.3390/catal11010030

Liu, N., *et al.* (2014) 'A review on TiO_2-based nanotubes synthesized via hydrothermal method: Formation mechanism, structure modification, and photocatalytic applications', *Catalysis Today*, *225*, pp. 34-51. doi: https://doi.org/10.1016/j.cattod.2013.10.090

Makeswari, M., and Saraswathi, P. (2020) 'Photo catalytic degradation of methylene blue and methyl orange from aqueous solution using solar light onto chitosan bi-metal oxide composite', *SN Applied Sciences*, *2*(3), p. 336. doi: https://doi.org/10.1007/s42452-020-1980-4

Mazumder, N. A., and Rano, R. (2018) 'Synthesis and characterization of fly ash modified copper oxide (FA/CuO) for photocatalytic degradation of methyl orange dye', *Materials Today: Proceedings*, *5*(1), 2281-2286. doi: https://doi.org/10.1016/j.matpr.2017.09.230

Mishra, P. K., Biswal, S. K., and Sahu, D. (2022) 'Synthesis and photocatalytic activity of Ni doped SnO_2 nanoparticles for removal of toxic industrial dyes', *Materials Today: Proceedings*, *68*, pp. 80-84. doi: https://doi.org/10.1016/j.matpr.2022.06.104

Mohajerani, A., *et al.* (2019) 'Nanoparticles in construction materials and other applications, and implications of nanoparticle use', *Materials*, *12*(19), p. 3052. doi: https://doi.org/10.3390/ma12193052

Parida, K. M. *et al.* (2008) 'Preparation, characterization, and photocatalytic activity of sulfate-modified titania for degradation of methyl orange under visible light', *Journal of colloid and interface science*, *318*(2), pp. 231-237. doi: https://doi.org/10.1016/j.jcis.2007.10.028

Peerakiatkhajohn, P. *et al.* (2021) 'Efficient and rapid photocatalytic degradation of methyl orange dye using Al/ZnO nanoparticles', *Nanomaterials*, *11*(4), p. 1059. https://doi.org/10.3390/nano11041059

Raliya, R. *et al.* (2017). Photocatalytic degradation of methyl orange dye by pristine titanium dioxide, zinc oxide, and graphene oxide nanostructures and their composites under visible light irradiation. *Applied Nanoscience*, *7*, pp. 253-259. doi: https://doi.org/10.1007/s13204-017-0565-z

Sasikala, R. *et al.* (2016) 'Photocatalytic degradation of trypan blue and methyl orange azo dyes by cerium loaded CuO nanoparticles', *Environmental Nanotechnology, Monitoring & Management*, *6*, pp. 45-53. doi: https://doi.org/10.1016/j.enmm.2016.07.001

Sinha, I., and De, A. K. (2020) 'An overview of synthesis techniques for preparing doped photocatalysts', *Nano-Materials as Photocatalysts for Degradation of Environmental Pollutants*, pp. 1-13. doi: https://doi.org/10.1016/B978-0-12-818598-8.00001-8

Slimani, Y. *et al.* (2023) 'Synthesis of Ce and Sm Co-doped TiO2 nanoparticles with enhanced photocatalytic activity for rhodamine B dye degradation', *Catalysts*, *13*(4), p. 668. doi: https://doi.org/10.3390/catal13040668

Subaihi, A., and Naglah, A. M. (2022) 'Facile synthesis and characterization of Fe_2O_3 nanoparticles using L-lysine and L-serine for efficient photocatalytic degradation of methylene blue dye', *Arabian Journal of Chemistry*, *15*(2), p. 103613. doi: https://doi.org/10.1016/j.arabjc.2021.103613

Sun, T., Qiu, J., and Liang, C. (2008) 'Controllable fabrication and photocatalytic activity of ZnO nanobelt arrays', *The Journal of Physical Chemistry C*, *112*(3), pp. 715-721. doi: https://doi.org/10.1021/jp710071f

Tabassum, H. *et al.* (2019) 'Recent advances in confining metal-based nanoparticles into carbon nanotubes for electrochemical energy conversion and storage devices. *Energy & Environmental Science*, *12*(10), pp. 2924-2956. doi: https://doi.org/10.1039/C9EE00315K

Tan, H. W. *et al.* (2019) 'Metallic nanoparticle inks for 3D printing of electronics', *Advanced Electronic Materials*, *5*(5), p. 1800831. doi: https://doi.org/10.1002/aelm.201800831

Tong, T. *et al.* (2008) 'Preparation of Fe3+-doped TiO2 catalysts by controlled hydrolysis of titanium alkoxide and study on their photocatalytic activity for methyl orange degradation', *Journal of Hazardous Materials*, *155*(3), pp. 572-579. doi: https://doi.org/10.1016/j.jhazmat.2007.11.106

Tran, V. A. *et al.* (2021) 'Solar-light-driven photocatalytic degradation of methyl orange dye over Co_3O_4-ZnO nanoparticles', *Materials Letters*, *284*, p. 128902. doi: https://doi.org/10.1016/j.matlet.2020.128902

Verma, M., Singh, K. P., and Kumar, A. (2020) 'Reactive magnetron sputtering based synthesis of WO_3 nanoparticles and their use for the photocatalytic degradation of dyes', *Solid State Sciences*, *99*, p. 105847. doi: https://doi.org/10.1016/j.solidstatesciences.2019.02.008

Wang, Z. *et al.* (2009) 'Highly photocatalytic ZnO/In_2O_3 heteronanostructures synthesized by a coprecipitation method', *The Journal of Physical Chemistry C*, *113* (11), pp. 4612-4617. doi: https://doi.org/10.1021/jp8107683

Yang, G., and Park, S. J. (2019) 'Conventional and microwave hydrothermal synthesis and application of functional materials: A review', *Materials*, *12*(7), p. 1177. doi: https://doi.org/10.3390/ma12071177

Zada, A. *et al.* (2022) 'Extended visible light driven photocatalytic hydrogen generation by electron induction from g-C3N4 nanosheets to ZnO through the proper heterojunction', *Zeitschrift für Physikalische Chemie*, *236*(1), pp. 53-66. doi: https://doi.org/10.1515/zpch-2020-1778

Zhang, L. *et al.* (2008) 'Nanoparticles in medicine: therapeutic applications and developments', *Clinical Pharmacology & Therapeutics*, *83*(5), pp. 761-769. doi: https://doi.org/10.1038/sj.clpt.6100400